ACS OMEGA

http://pubs.acs.org/journal/acsodf

Article

Mechanistic Study on the Decrease in Injectivity during Salt-Resistant Polymer Flooding

Tongchun Hao, Liguo Zhong,* Jianbin Liu, Hongyu Sun, Tianyin Zhu, Hailong Zhang, and Shaojie Wu

Cite This: *ACS Omega* 2022, 7, 11293−11304

Read Online

ACCESS | Metrics & More | Article Recommendations

ABSTRACT: According to numerous laboratory experiments and field applications, polymer flooding can effectively modify the liquid absorption profile and increase the sweep efficiency, thereby enhancing the oil recovery. However, long-term injection of polymers decreases the effective permeability of the reservoir and plugs the formation pores, resulting in irreversible reservoir damage. In the development process, polymer types and concentrations must be selected according to the reservoir to avoid problems such as plugging of the formation pores. This study was aimed at clarifying the degree of plugging and the injection limit of the reservoir when a salt-resistant polymer (SRP) is used in production processes of the Daqing Oilfield. To this end, oil displacement experiments, dynamic and static adsorption experiments, and SEM observations were performed using representative reservoir fluid and core samples. The static adsorption of "medium-molecular" SRP reached equilibrium after 36 h, and the saturated adsorption capacity was 3.56 mg/g, which was approximately 2−5 times the dynamic adsorption capacity. For medium-molecular SRP, with a molecular mass of 7 million, the lower limit of the core permeability was 20−40 mD. When the permeability was less than 100 mD, the SRP concentration injected into the core could not exceed 900 mg/L. The oil displacement capacity of SRP decreased owing to the macromolecular hydration radius and the strong aggregation effect of SRP. Polymer adsorption and the retention of sand-carrying critically decreased water permeability. This study provides insights into SRP flooding under different geological conditions in the Daqing Oilfield and can help clarify the molecular mass and concentration of polymers with changes in the reservoir conditions.

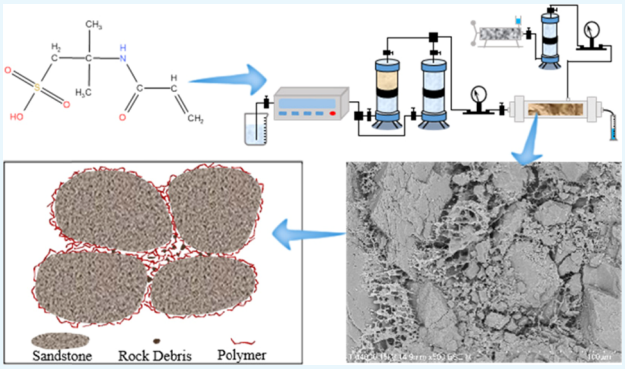

INTRODUCTION

The development of oil resources is influenced by a variety of elements, such as the oil and gas reserves, types of oil and gas, geological conditions, and development stage.[1] Water can be injected into the formation as an inexpensive and simple flooding agent to replenish the formation energy and push crude oil through piston action. However, reservoirs are heterogenous, and high-permeability reservoirs exhibit low seepage resistance. The high-permeability layer absorbs more liquid than the medium and low permeability layers under the same injection pressure. This phenomenon gradually intensifies with the injection time until the injection of water in the high-permeability layer is inefficient or even ineffective.[2] The recovery of water flooding depends on the swept volume and oil displacement efficiency. The oil recovery and oil displacement efficiency can be increased at a certain swept volume. Consequently, most oil fields introduce chemical reagents to lower the permeability of the high-permeability layer and enhance the oil displacement efficiency to increase the oil recovery.[3] Polymer flooding, as a representative EOR technique, is extensively employed in many oilfields, owing to its wide range of material sources, easy synthetic methods, high oil displacement efficiency, and low cost.[4,5] Following injection, the polymer can selectively seal the high-permeability zone and lower its permeability. At a constant injection rate, the injection pressure increases throughout the well, increasing the adsorption differential pressure and liquid absorption volume in the medium- and low-permeability zones. This framework is typically appropriate for reservoirs with high oil saturation and medium heterogeneity. China conducted field testing of polymer flooding in the oilfields of Daqing, Dagang,[6] Liaohe,[7] and Shengli[8] and obtained exceptional stimulation results. However, after the polymer enters the low- and medium-permeability layers, it remains in those layers, thereby increasing the permeability resistance.[9] The increase in permeability resistance is substantially greater than that of the high-

Received: January 15, 2022
Accepted: February 28, 2022
Published: March 21, 2022

ACS Publications

© 2022 The Authors. Published by American Chemical Society

https://doi.org/10.1021/acsomega.2c00296
ACS Omega 2022, 7, 11293−11304

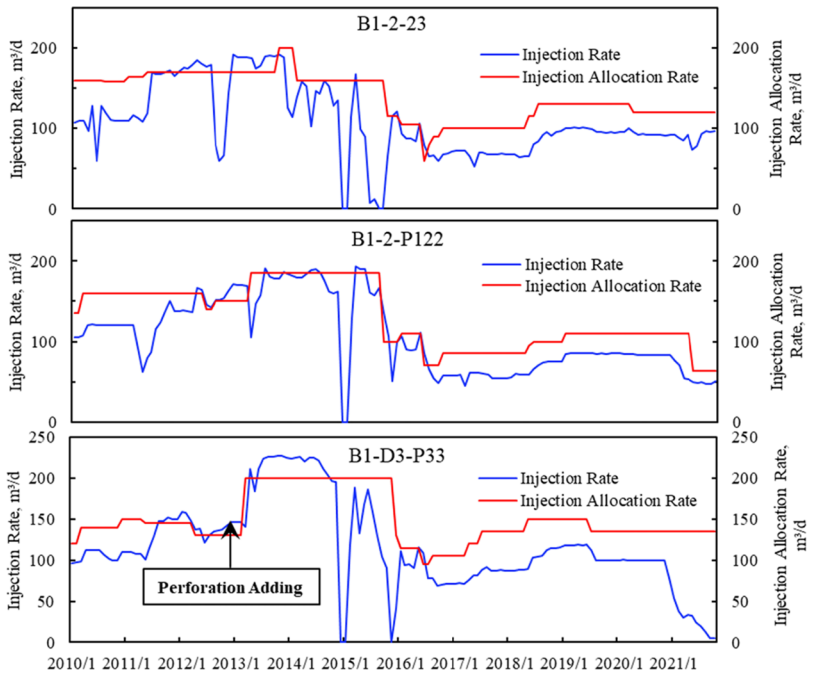

Figure 1. Decrease in the injectivity of polymer injection wells in the Daqing Oilfield.

permeability layer for the same injection volume. The injection pressure increases with the amount of adsorbed polymer in the reservoir.[10−12] To prevent polymer loss owing to reservoir fractures, the injection pressure must be lower than the fracturing pressure. Consequently, in the case of continuous polymer injection, once the injection pressure exceeds the top limit, the adsorption pressure difference in each layer at the injection end progressively decreases, and the injectivity of the polymer injection well gradually diminishes and even approaches zero. For example, in the case of the Daqing Oilfield, the reservoir permeability is usually less than 200 mD. The injection rate of most polymer injection wells was lower than the injection allocation rate for several years and decreased significantly after production (Figure 1), increasing the cost of polymer flooding and decreasing the economic effect of polymer flooding to enhance oil recovery. Although nanoparticles can be mixed with polymers to alleviate this problem, large-scale roll-out remains a distant possibility.[13,14]

The decrease in the polymer injectivity can be primarily attributed to polymer obstruction in pipelines and formation during polymer flooding.[15−17] The location and mechanism of plugging in the polymer flooding process have been examined to increase the polymer flooding efficiency and design a polymer flooding reservoir plugging system. Clogging may occur in the polymer flooding process owing to several reasons. "Fisheye" scaling may occur near the well area of the polymer injection well because of the low solubility of the dry polymer powder or deviation in the construction means.[18−20] Adsorption and trapping of injected polymers in the reservoir, particularly at tiny pore openings, can limit the reservoir permeability.[21−24] The water used to manufacture the polymer may be incompatible with formation water, resulting in inorganic scaling. Moreover, the polymer may be stranded in the oil layer winding, generating large obstruction and limiting the progress of polymer flooding. SRB bacteria in water can proliferate using polymers as an energy source, resulting in bacterial obstruction and inorganic scale blockage if the injected water quality is not adequately high.[25−27] The existing studies mainly focused on theoretically analyzing the mechanism of plugging formation. However, the compatibility of polymer and reservoir conditions is a key factor influencing the occurrence of plugging in the polymer flooding process in oil fields.[28−30] Consequently, it is crucial to investigate the injectivity of the polymer utilized in each oil field under the appropriate reservoir geological circumstances and polymer compatibility with the formation conditions and degree of plugging.[31]

This study was aimed at clarifying the degree of reservoir plugging and the injection limit for the case in which a salt-resistant polymer (SRP) is used in the Daqing Oilfield. To this end, the injection ability of SRPs with different molecular weights and concentrations for different types of cores and permeability conditions was simulated by displacement experiments. The main factors influencing the adsorption capacity of the SRP were determined by measuring the adsorption retention of polymers in porous media in dynamic and static conditions. The mechanism of the decrease in the polymer injection ability was analyzed from the aspects of the polymer molecular size, aggregation state, and adsorption. This research can provide a basis for the optimal molecular weight and concentration of polymers for the SRP flooding of reservoirs in the Daqing Oilfield and theoretical guidance for the study of plugging systems.

EXPERIMENTAL MATERIALS AND METHODS

Materials. The polymer solution used in this study was a "medium-molecular" SRP with a molecular mass of 700×10^4. The polymer structure is shown in Figure 2. The polymer is a product provided by the Daqing Oilfield and has a commercial application value. Moreover, the high-molecular partially hydrolyzed polyacrylamide (PHPAM) with a molecular mass of 14×10^4 and ultrahigh-molecular PHPAM with a molecular mass of 25×10^4 were used. The sand sample was a natural core sand sample from the Gaotaizi Reservoir (more than 40 mesh). Crude oil with a viscosity of 6.0 mPa·s was derived from the

https://doi.org/10.1021/acsomega.2c00296
ACS Omega 2022, 7, 11293−11304

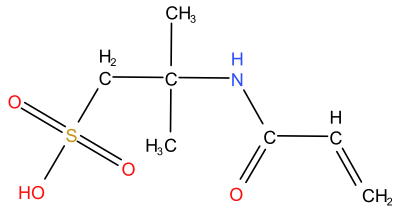

Figure 2. Molecular structure of the salt-resistant polymer.

Daqing Gaotaizi oilfield. The water samples included samples of clean injection water and deeply treated sewage from the Daqing Oilfield. Tables 1, 2 summarize the water quality analysis results. The sizes of the artificial and natural cores are 25 × 100 mm and 25 × 100 mm (70−100 mm), respectively. The reservoir temperature in the Daqing Oilfield is approximately 45 °C; therefore, the experimental temperature was set as 45 °C.

Methods. *Preparation of Polymer Solution.* The medium-molecular SRP solution was sheared with clear water to prepare a 5000 mg/L polymer mother solution, and the shear duration was measured at a viscosity retention rate of 60%. The other two polymer solutions were sheared at the same rate and the same duration. Subsequently, a 75-mesh filter was used to filter the polymer solution. Finally, the oilfield effluent was used to dilute the polymer mother solution to the target concentration of 900 mg/L.

Polymer Flooding Experiment. The changes in the pressure of artificial cores with different permeability levels during water flooding, polymer flooding, and subsequent water flooding were measured through an indoor core simulation experiment at a polymer solution concentration of 900 mg/L, and the resistance coefficient and residual resistance coefficient were calculated. The following steps were adopted:

1) Device connection: using the appropriate method, connect the flooding device, pressure detection device, and generated-liquid collection device; check for air and liquid leakage at each point; and verify that no leaking point exists.
2) Core vacuuming: after drying, weigh the core and attach it to the vacuuming apparatus. Initiate the timer when the vacuum gauge on the vacuum pump decreases to less than 0.098 MPa, and vacuum the core constantly. For an artificial homogenous long core and a natural core, the vacuuming time must be 8 h and at least 5 h, respectively.
3) Water saturation: seal the outlet end of the valve, connect the inlet end of the valve to the acid burette, slowly inject saturated water into the core, gradually open the outlet end of the valve, and swiftly close the valve when water flows out. Track the amount of injected water.
4) Water permeability measurement: vary the flooding rates, inject the simulated formation water into the core at a consistent rate, record the stable pressure difference, and use Darcy's law to compute the effective core permeability.
5) Crude oil saturation: replace the core with simulated oil until the water yield is zero and record the amount of saturated oil at this point.
6) Water injection: inject water at a steady rate, shift the core to the desired water production rate, and record the injection pressure, oil production rate, and liquid production rate.
7) Polymer injection: perform a constant speed injection of 6.0 PV polymer solution. Monitor the injection pressure, oil production rate, and liquid production rate, and obtain samples of the generated fluid at regular intervals to determine the polymer content.
8) Subsequent water flooding: continue to infuse 6.0 PV water at a steady pace and record the injection pressure, oil production rate, and liquid production rate.

The resistance coefficient and residual resistance coefficient are technical indicators that specify the quantity of polymer retained in a porous medium. These parameters can be mathematically represented as follows:

$$F_R = \frac{\Delta P_2}{\Delta P_1} \quad (1)$$

$$F_{RR} = \frac{\Delta P_3}{\Delta P_1} \quad (2)$$

where F_R is the resistance coefficient; F_{RR} is the residual resistance coefficient; ΔP_1 is the difference in the water drive pressure; ΔP_2 is the difference in the polymer flooding pressure; and ΔP_3 is the differential pressure in the subsequent water flooding.

The F_R and F_{RR} test flow and experimental equipment are illustrated in Figure 3. The experimental equipment included advection pumps, pressure sensors, core grippers, hand pumps, and intermediate vessels. Parts other than the advection pump and the hand pump were maintained at a temperature at 45 °C in a constant temperature box. The system error of the experiment included the instrument error of the injection pump, intermediate vessel, and pressure gauge, and the same set of experimental equipment was used in the experimental process to minimize the influence of the system error on the experimental results. The characteristics of artificial cores used in various core permeability studies are listed in Table 3.

The system errors of this experiment included instrument errors such as those of the injection pumps, intermediate containers, and pressure gauges. The same set of experimental equipment was used in the experiment to minimize the influence of system errors on the experimental results.

Polymer Adsorption Experiment. The physicochemical interaction between the polymer and formation rock and fluid is critical in the effective implementation of polymer flooding and chemical flooding with the polymer as the principal agent. Static and dynamic adsorption tests were performed based on the polymer adsorption theory. The adsorption behavior of the SRP solution on the natural core and dynamic retention characteristics in porous media were investigated, and the adsorption process and variables influencing the polymer solution were examined.

Static Adsorption. *Experimental Procedure.*

Table 1. Water Quality Analysis of Clean Water

ions	Ca^{2+}	Mg^{2+}	Cl^-	HCO_3^-	CO_3^{2}	SO_4^{2-}	$K^+ + Na^+$	total
concentration (mg/L)	45.69	29.18	124.11	512.5	0	5.76	168.82	886.06

https://doi.org/10.1021/acsomega.2c00296
ACS Omega 2022, 7, 11293−11304

Table 2. Water Quality Analysis of Deeply Treated Sewage Samples

ions	Ca^{2+}	Mg^{2+}	Cl^-	HCO_3^-	CO_3^{2}	SO_4^{2-}	$K^+ + Na^+$	total
concentration (mg/L)	20.07	6.08	999.69	2020.37	103.22	6.0	1378.51	4533.91

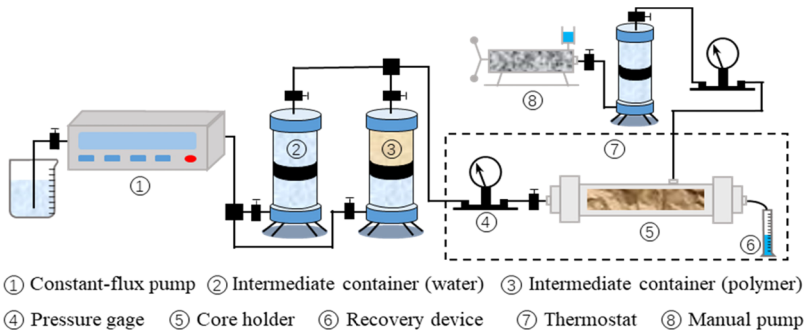

Figure 3. Schematic of core flooding experimental equipment and process.

Table 3. Design Scheme of the Polymer Core Flooding Experiment

polymer			core			
molecular mass ($\times 10^4$)	viscosity (mPa s)	concentration (mg/L)	pore volume	porosity (%)	permeability (mD)	type
700	52.6	600	8.05	16.4	45.2	artificial core
			10.94	22.3	94.6	
			11.82	24.1	296	
		900	6.87	14.0	22.5	
			7.85	16.0	40.9	
			9.96	20.3	62.7	
			11.68	23.8	110.6	
			12.02	24.5	310.5	
			11.43	23.3	108.3	natural core
			12.90	26.3	315.2	
			13.69	27.9	489.6	
		1200	8.05	16.4	43.5	artificial core
			10.84	22.1	85.2	
			12.71	25.9	284	
1400	24.7	900	6.92	14.1	19.5	
			7.95	16.2	42.4	
			10.79	22.0	69.2	
			11.38	23.2	103.8	
2500	36.2		7.16	14.6	24.8	
			8.10	16.5	45.7	
			10.40	21.2	65.9	
			12.12	24.7	114.2	

1) Certain amounts of core sand and the polymer solution were added to a tapered bottle with a plug, and the overall weight of the conical bottle was recoded.
2) For a certain period, the conical bottle was placed in an incubator at 45 °C. The conical flask was oscillated at regular intervals to ensure that the adsorbent was completely immersed in the solution.
3) The solution was shaken in the conical container and poured into the centrifugal tube. The samples were centrifuged for 30 min at 3000−4000 rpm. Subsequently, using the absorbance method, the polymer concentration in the clear liquid was measured three times, and the results were averaged.

Variation in the Adsorption Capacity of the Polymer Solution with Time. The reservoir temperature (45 °C) in the Gaotaizi polymer flooding test region was simulated, and the adsorption capacity at various adsorption durations was determined using a natural core under a constant liquid−solid ratio. The durations of the trial were 12, 24, 36, and 48 h.

Static Adsorption of Polymer Solutions at Different Liquid−Solid Ratios. The reservoir temperature (45 °C) was simulated in the Daqing polymer flooding test area, natural cores were used to assess the static adsorption capacity at various liquid−solid ratios, and the corresponding liquid−solid ratio was determined at a steady adsorption capacity. The liquid to solid ratios were 3, 5, 10, 15, and 20 mg/L, with a standing time of 36 h.

Static Adsorption of Polymer Solutions with Different Concentrations. The static adsorption capacity of three polymer solutions with concentrations of 300, 600, 900, 1200, and 1500 mg/L was measured using natural cores at a temperature of 45 °C.

Dynamic Adsorption. Experimental Method. The sand-filled tube core with a diameter of 2.5 cm and length of 10 cm

https://doi.org/10.1021/acsomega.2c00296
ACS Omega 2022, 7, 11293−11304

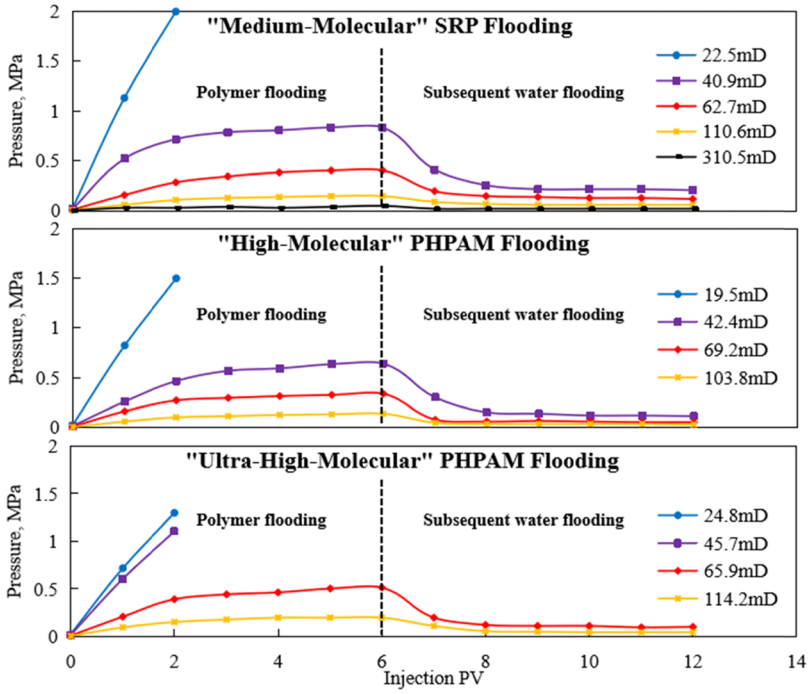

Figure 4. Injection pressure curves of different polymers in cores with different permeabilities.

Table 4. F_R and F_{RR} after Polymer Solution Flooding (Cp = 900 mg/L)

polymer	viscosity (mPa s, 10 s^{-1})	permeability ($\times 10^{-3}$ μm^2)	resistance coefficient (F_R)	residual resistance coefficient (F_{RR})	decrease in the permeability (%)
medium-molecular SRP	52.6	22.5	blocking	blocking	100
		40.9	50.1	12.4	92.0
		62.7	38.3	11.2	91.4
		110.6	24.6	9.8	89.7
		310.5	20.5	8.2	87.8
high-molecular PHPAM	24.7	19.5	blocking	blocking	100
		42.4	40.1	7.2	86.2
		69.2	35.6	5.7	83.2
		103.8	22.4	4.9	80.6
ultrahigh-molecular PHPAM	36.2	24.8	blocking	blocking	100
		45.7	blocking	blocking	100
		65.9	50.3	10.0	90.1
		114.2	33.0	7.6	86.7

was dried and weighed to saturate the formation water, and the permeability of the formation water was measured. The polymer solution was injected at a flow rate of 1 mL/min, and the produced polymer concentration was measured until it was equal to that of the injected polymer. The formation water was injected at a constant rate, and samples were collected from the core outlet until no polymer was detected in the core-produced fluid.

Using the material balance approach, the quantity of the polymer retained in the formation was estimated using eq 3.

$$Q = \left(\rho_0 V_0 - \sum_{i=1}^{n} \rho_i V_i\right)/W \tag{3}$$

where Q is the polymer retained in the core, μg/g; ρ_0 is the injected polymer solution concentration, mg/L; V_0 is the cumulative volume of the injected polymer solution, mL; ρ_i is the polymer concentration of the ith outflow sample at the core outlet, mg/L; V_i is the volume of the ith outflow sample, mL; n is the number of outflow samples collected at the core outlet; and W is the core dry mass, g. The error in the polymer dynamic and static adsorption experiment was mainly the mass measurement error. The electronic balance used in the experiment was accurate to 10^{-4} mg, which satisfied the experimental requirements.

The error in the polymer dynamic and static adsorption experiment was mainly the mass measurement error. The electronic balance used in the experiment was accurate to 10^{-4} mg, which satisfied the experimental requirements.

Experimental Design. The reservoir temperature (45 °C) in the Gaotaizi polymer flooding test region was simulated. Natural cores with permeabilities of 100, 300, and 500 mD were used to perform flooding tests with the medium-molecular SRP with a polymer solution concentration of 900 mg/L. The dynamic adsorption capacity was investigated at various adsorption periods.

https://doi.org/10.1021/acsomega.2c00296
ACS Omega 2022, 7, 11293−11304

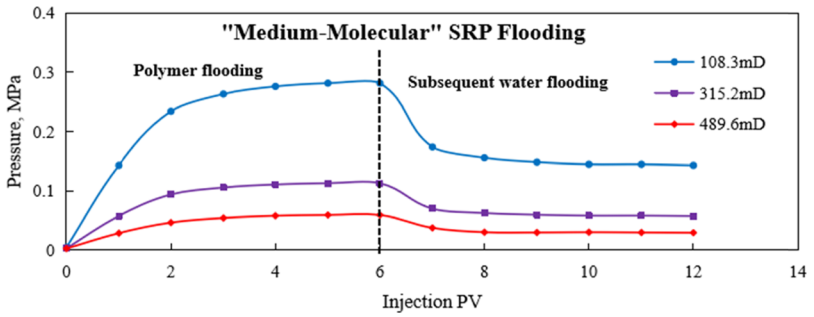

Figure 5. Medium-molecular SRP flooding with different permeability natural core injection pressures.

Table 5. F_R and F_{RR} of Natural Core Displaced by Medium-Molecular SRP (Cp = 0.9 g/L)

polymer	viscosity (mPa·s, 10 s^{-1})	permeability ($\times 10^{-3}$ μm^2)	resistance coefficient (F_R)	residual resistance coefficient (F_{RR})	decrease in the permeability (%)
medium-molecular SRP	52.6	108.3	66.8	33.8	97.0
		315.2	44.7	22.6	95.5
		489.6	26.8	13.2	92.5

Table 6. F_R and F_{RR} of the Long Core Displaced by the Medium-Molecular SRP

permeability level (mD)	polymer concentration (mg/L)	permeability ($\times 10^{-3}$ μm^2)	EOR (%)	resistance coefficient (F_R)	residual resistance coefficient (F_{RR})	decrease in the permeability (%)
300	600	296	8.80	9.36	4.1	75.60
	900	310.5	14.60	20.5	8.2	87.80
	1200	284	19.20	31.7	11.6	91.38
100	600	94	6.50	20.8	9.0	88.90
	900	110.6	8.80	24.6	9.8	89.70
	1200	85.2	10.30	33.1	13.1	92.40
50	600	45	4.30	38.2	12.0	91.69
	900	40.9	5.90	50.1	12.4	92.00
	1200	43.5	7.50	55.8	15.2	93.42

RESULTS AND DISCUSSION

Polymer Flooding Experiment. *Formation Permeability. Artificial Core.* Flooding experiments were conducted using artificial cores with different permeabilities, and the polymer concentration was 900 mg/L. Figure 4 shows the change in the pressure at the injection end recorded during the experiment. Since the polymer injection, the pressure at the injection end rapidly increased, and after the injection of approximately 2 PV of polymer, the pressure increase rate at the injection end decreased and stabilized. This phenomenon occurred owing to the high viscosity of the polymer solution, which generated high resistance when it flowed in the pores. When the polymer solution first appeared from the outlet end, it occupied the high-permeability pores in the core. As the polymer solution continuously enters the low-permeability pores, the pressure at the injection end gradually increases until the polymer solution occupies all the pores. After subsequent water flooding was initiated, the pressure at the injection end rapidly decreased. After 1 PV of water was injected, the pressure at the injection end gradually decreased and stabilized. However, the polymer molecules were adsorbed on the surface of the sand particles, resulting in a higher pressure at the injection end after subsequent water flooding than that during the previous water flooding.

The calculated resistance coefficient (FR), residual resistance coefficient (FRR), and decrease in the core permeability for each group of experiments are presented in Table 4. The FR of the medium-molecular SRP is larger than that of the high-molecular PHPAM but smaller than that of the ultrahigh-molecular PHPAM. Under the same permeability conditions, the resistance coefficient was not proportional to the molecular weight of the polymer but proportional to the apparent viscosity in the porous medium. This phenomenon occurred because during the flow of the polymer, the stretching effect was dominant, resulting in an increased apparent viscosity and FR. Table 4 indicates that the FRR of the SRP ranged between 8 and 12, whereas that of the PHPAM was less than 10. Under the same permeability conditions, the FRR of the medium-molecular SRP was higher than that of the high-molecular PHPAM and ultrahigh-molecular PHPAM. In other words, the retention capacity of the SRP was higher than that of the PHPAM. Experiments demonstrated that polymer adsorption and retention in the core was irreversible, thereby decreasing the core permeability. The core permeability decreased by 92.0% when the 40.9 mD core was displaced by the medium-molecular SRP solution, and the displacement of the 22.5 mD core led to core plugging. Therefore, the lower limit of the permeability of the medium-molecular SRP solution-flooded core was 20−40 mD. In general, when choosing the SRP, the formation permeability must be determined in accordance with the polymer solution; otherwise, the formation may be irreversibly damaged.

Natural Core. High-permeability and medium−low permeability channels coexist in natural cores, and the degree of mineral cementation is not uniform, which renders the pore structure complex. Therefore, core flooding experiments must be performed using natural cores with different permeability

https://doi.org/10.1021/acsomega.2c00296
ACS Omega 2022, 7, 11293−11304

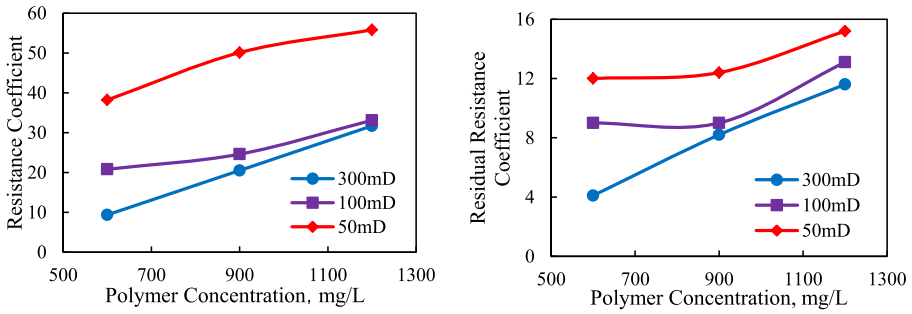

Figure 6. F_R and F_{RR} of polymer flooding of cores with different permeabilities.

Table 7. Polymer Solution Standing for Different Time Adsorption Capacities

polymer	time (h)	absorbance	concentration loss (mg/L)	adsorption quality (mg)	sand quality (g)	adsorption capacity (mg/g)
medium-molecular SRP	12.00	0.37	151.00	6.04	4.00	1.51
	24.00	0.35	225.00	9.00	4.00	2.25
	36.00	0.35	328.13	13.13	4.00	3.28
	48.00	0.34	356.25	14.25	4.00	3.56
high-molecular PHPAM	12.00	0.48	71.05	2.84	4.00	0.71
	24.00	0.45	153.00	6.12	4.00	1.53
	36.00	0.40	260.53	10.42	4.00	2.61
	48.00	0.39	276.32	11.05	4.00	2.76
ultrahigh-molecular PHPAM	12.00	0.44	48.57	1.94	4.00	0.49
	24.00	0.39	172.00	6.88	4.00	1.72
	36.00	0.35	267.14	10.69	4.00	2.67
	48.00	0.33	288.00	11.52	4.00	2.88

values. Figure 5 shows the variation in the injection end pressure in the displacement experiment based on natural cores. The calculated resistance coefficient, residual resistance coefficient, and decrease in the permeability are presented in Table 5. No obvious blockage occurred during the flooding process; however, after subsequent water flooding, core permeability decreased by more than 90%. The resistance coefficient and the residual resistance coefficient were two and three times larger than those of the artificial core with the same level of permeability, respectively. This finding indicated that the complex hole roar conditions in the natural core increased the difficulty of polymer injection, and SRP was more likely to be retained in the natural core.

Polymer Concentration. The polymer concentration considerably influences the perceived viscosity of the polymer. SRP flooding simulation studies with various quantities of medium-molecular SRP were performed. The F_R, F_{RR}, and decrease in the permeability for core flooding with different polymer concentrations and permeabilities are shown in Table 6 and Figure 6. The intermolecular entanglement intensified as the polymer concentration increased, and the network topology became more compact. The injection pressure increased during the flooding process, and a larger amount of polymer remained in the rock. Increasing the polymer intermolecular force increased the adsorption but did not lead to obstruction.

The F_R and F_{RR} values of the 300 and 100 mD cores were only slightly different, but those of the 50 mD low-permeability cores were considerably greater than those of the 100 and 300 mD high-permeability cores. Decreasing the polymer concentration did not considerably decrease the injection pressure of polymers in low-permeability formations, although the polymer viscosity decreased. In addition to the influencing factors, specifically, the polymer adsorption and high viscosity, the consistency between the polymer molecular size and the rock pore size (particularly, the pore throat) considerably influenced polymer molecular retention.

In general, decreasing the polymer solution concentration can decrease the injection pressure of polymer flooding, which influences the microscopic oil displacement efficiency of polymer flooding. Consequently, to achieve the highest oil flooding efficiency, a suitable polymer concentration must be used. The suitable polymer concentration of cores with varying permeability can be preliminarily calculated using Figure 6. When the permeability is less than 100 mD, the SRP concentration injected into the core must not be greater than 900 mg/L; otherwise, the injectivity would considerably decrease.

Polymer Adsorption Experiment. *Static Adsorption. The Adsorption Capacity of the Polymer Solution Changes with Time.* The outcome of the static adsorption capacity assessment of polymers is the maximum adsorption capacity after adsorption equilibrium. SRP with a concentration of 900 mg/L was utilized to measure the adsorption capacity measurement at different periods to evaluate the adsorption equilibrium time of SRP with varying molecular weights. Table 7 and Figure 7 show the experimental outcomes. At the start of the experiment, the static adsorption capacity of the three polymers steadily increased. The static adsorption capacity of the three polymers was steady when the standing time exceeded 36 h; therefore, the adsorption equilibrium time of the SRP was determined to be 36 h.

Static Adsorption of Polymer Solutions at Different Liquid−Solid Ratios. Figure 8 presents the static adsorption values of polymer solutions at various liquid−solid ratios. In the static adsorption experiment, the polymer adsorption capacity increased with the liquid−solid ratio. The adsorption capacity of polymers with a low and high liquid−solid ratios significantly decreased. As the liquid−solid ratio increased, the static

https://doi.org/10.1021/acsomega.2c00296
ACS Omega 2022, 7, 11293−11304

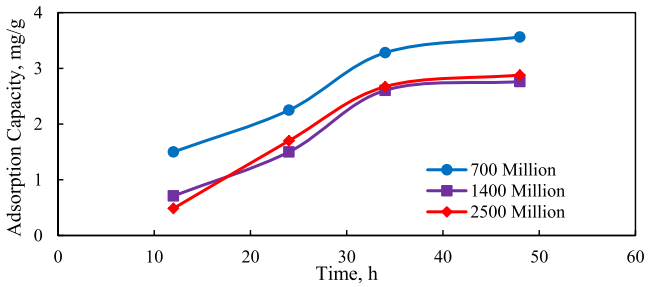

Figure 7. Temporal variation in the adsorption capacity of polymers with different molecular weights and concentration of 900 mg/L.

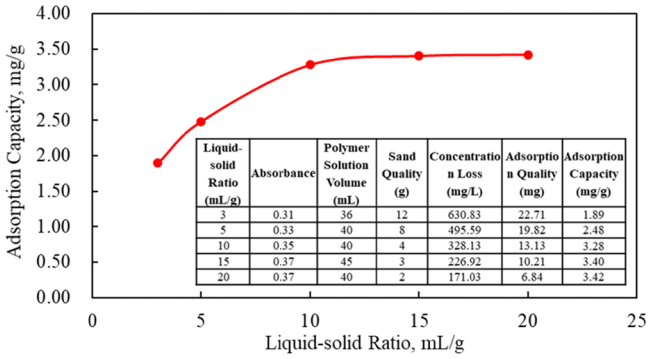

Liquid-solid Ratio (mL/g)	Absorbance	Polymer Solution Volume (mL)	Sand Quality (g)	Concentration Loss (mg/L)	Adsorption Quality (mg)	Adsorption Capacity (mg/g)
3	0.31	36	12	630.83	22.71	1.89
5	0.33	40	8	495.59	19.82	2.48
10	0.35	40	4	328.13	13.13	3.28
15	0.37	45	3	226.92	10.21	3.40
20	0.37	40	2	171.03	6.84	3.42

Figure 8. Polymer adsorption capacity at different liquid−solid ratios.

adsorption capacity progressively increased and stabilized. When a suitable polymer solution was used, the static adsorption capacity of the sand particles was limited by their surface area.

Static Adsorption of Polymer Solutions with Different Concentrations. Table 8 presents the statistical experimental data of polymer solutions with different concentrations after standing for 36 h, and Figure 9 shows the isothermal static adsorption curve of polymer solutions with different concentrations. When the polymer concentration increased from 300 to 900 mg/L, the static adsorption capacity of the polymer increased. When the polymer concentration exceeded 900 mg/L, because of the limitation of the solid−liquid ratio, the static adsorption amount saturated and did not increase with the polymer concentration. At different concentrations, the adsorption capacity of the medium-molecular ASPAM was greater than that of high-molecular and ultrahigh-molecular PHPAM. This phenomenon occurred because the molecular chain of medium-molecular ASPAM was shorter than those of the other two polymers and could thus enter the finer pore roar and be adsorbed in the pores. The adsorption loss of the polymer could be decreased by decreasing the polymer solution concentration, and the injection pressure of the polymer solution could be decreased. However, the effect of decreasing the concentration on the viscosity of the polymer entering the reservoir must be considered.

Dynamic Adsorption. The dynamic adsorption capacity test results of the polymer solution are shown in Table 9. Table 9 shows that the static adsorption capacity of the medium-molecular SRP is approximately 2−5 times that of the dynamic adsorption capacity. This phenomenon could be attributed to the fluid shearing effect in the dynamic adsorption. The chains are shorter, and the intertwining phenomenon weakens. Consequently, the adsorption capacity is less than that in the static adsorption. Sameer Al-Hajri highlighted the large difference in the static and dynamic adsorption amounts of various polymers in the core.[9] For a given type and concentration of the polymer solution, lower core permeability corresponds to a smaller pore size and larger dynamic adsorption capacity. Because the molecular structure of the polymer does not change, the polymer adsorption capacity on the surface of the medium does not change, although the spatial structure formed by its entanglement increases the adsorption layer thickness. The external force balance is the main factor affecting the dynamic adsorption capacity. The small size of the pore throat increases the entanglement force between the SRP molecules in the pores, which leads to the thickening of the adsorption layer.

The polymer solution retention varies with the rock permeability, polymer type, concentration, and displacement rate.[32] Manichand and Seright reported that polymer retention values exceeding 0.2 mg/g may influence the oil displacement rate and economics of the polymer flooding process.[33] Therefore, this experiment demonstrated that the use of SRP was not economical.

Analysis of the Mechanism of Decrease in the Polymer Injection−Production Capacity. *Polymer Molecular Size.* The degree of matching between the polymer molecular size and the core pore size is a key factor influencing the polymer

Table 8. Static Adsorption Capacity of Polymer Solutions with Different Concentrations

polymer	initial concentration (mg/L)	absorbance	concentration loss (mg/L)	adsorption quality (mg)	sand quality (g)	adsorption capacity (mg/g)
medium-molecular SRP	300.00	0.23	131.25	5.25	4.00	1.31
	600.00	0.30	204.17	8.17	4.00	2.04
	900.00	0.35	328.13	13.13	4.00	3.28
	1200.00	0.43	350.00	14.00	4.00	3.50
	1500.00	0.51	357.29	14.29	4.00	3.57
high-molecular PHPAM	300.00	0.22	138.95	5.56	4.00	1.39
	600.00	0.34	173.68	6.95	4.00	1.74
	900.00	0.45	260.53	10.42	4.00	2.61
	1200.00	0.57	295.26	11.81	4.00	2.95
	1500.00	0.69	303.95	12.16	4.00	3.04
ultrahigh-molecular PHPAM	300.00	0.19	47.14	1.89	4.00	0.47
	600.00	0.29	157.14	6.29	4.00	1.57
	900.00	0.39	267.14	10.69	4.00	2.67
	1200.00	0.51	298.57	11.94	4.00	2.99
	1500.00	0.65	314.29	12.57	4.00	3.14

https://doi.org/10.1021/acsomega.2c00296
ACS Omega 2022, 7, 11293−11304

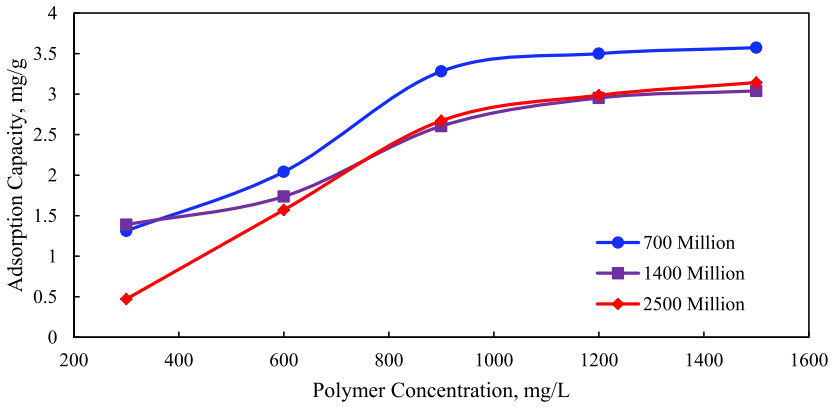

Figure 9. Static adsorption capacity of the polymer solution (36 h).

Table 9. Dynamic Adsorption Capacity of Medium-Molecular SRP (Cp = 900 mg/L)

polymer	permeability (10^{-3} μm^2)	polymer concentration (mg/L)		injection polymer volume (mL)	core quality (g)	adsorption capacity (mg/g)
		injection	Production			
medium-molecular SRP	107.9	900	462.42	238.2	87.1	1.20
	328.6	900	506.25	186.0	73.9	0.99
	507.9	900	562.50	166.7	72.7	0.77

Table 10. Characteristic Parameters of the Experimental Polymer

polymer	molecular mass ($\times 10^4$)	intrinsic viscosity (dL/g)	molecular cyclotron radius (μm)	decrease in the permeability			
				50 mD	100 mD	200 mD	500 mD
medium-molecular SRP	700	40.4	0.19	56.8%	43.7%	32.2%	19.7%
high-molecular PHPAM	1400	33.6	0.22	59.2%	46.3%	34.3%	21.7%
ultrahigh-molecular PHPAM	2500	48.0	0.31	70.5%	58.3%	45.4%	33.2%

injectivity. According to Flory's theory of polymer solutions, the cyclotron radius (or hydraulic radius) of polymer molecules in the polymer solution can be calculated using the following formula:[34,35]

$$r_p = 0.62 \times 10^{-4}([\eta]M)^{1/3} \quad (4)$$

where $[\eta]$ is the characteristic viscosity of the polymer in an aqueous solution, mL/g; M is the molecular mass of the polymer, $\times 10^4$; and α is a constant, $\alpha = (10/3)\pi N\xi^3$, which is approximately 4.22×10^{24}.

The characteristic parameters of several polymers used in the experiment are listed in Table 10. The medium-molecular SRP exhibited a large molecular cyclotron radius of 0.19 μm, and the core permeability decreased when the thickness of the polymer hydration adsorption layer increased. For high platform cores with an average permeability of 100 mD, the permeability decreased by 43.7%. Moreover, the same thickness of the polymer adsorption layer had different effects on the decrease in the core permeability with different permeabilities, especially for low permeability cores (permeability less than 50−100 mD).

Polymer Aggregation State. At present, polymer solutions for oil flooding represent subconcentrated solution systems, and their application concentrations range between those of dilute polymer solutions and concentrated solutions. The intermolecular interactions of PHPAM and other common polymers are mainly physical entanglement, while the intermolecular interactions of the SRP include fan forces, hydrogen bonds, and intermolecular associations in addition to intramolecular friction. The SRP solution viscosity is superior to that of ordinary polymers because of strong intermolecular interactions. Figure 10 shows the SEM images of the SRP and PHPAM solutions. Figure 10a,c show the initial sample of 900 mg/L medium-molecular SRP and high-molecular PHPAM, respectively. The SRP molecules exhibit considerable aggregation, and the aggregate size of the polymer groups can reach 5−10 μm, significantly exceeding the pore radius of the rock. However, normal polymers do not exhibit significant aggregation, and the polymer molecules are evenly distributed. Figure 10b,c show samples of the 900 mg/L medium-molecular SRP and ordinary polymer after shearing, respectively. After shear action, the polymer group is destroyed, the order is weakened, and the entanglement and aggregation of polymer molecules are enhanced. However, the cementation remains high. In contrast, the polymer molecules become more disordered after shearing and cannot maintain their basic morphology. Therefore, the viscosity of the SRP is significantly higher than that of the PHPAM after high-strength mechanical shearing, which also influences the seepage characteristics of the solution in porous media.

Influence of Polymer Adsorption on the Polymer Injectivity. The polymers are characterized by a high molecular weight and long chain morphology. These chains contain many polar groups that attach the rock surface through van der Waals forces and hydrogen bonding available on the pole.[33] This phenomenon decreases the number of polymer molecules in the polymer solution, which decreases the polymer solution concentration and increases the entropy of the polymer solution. Conversely, the entropy reduction is due to the loss of polymer freedom upon adsorption on the surface.[9] Essentially, polymers

https://doi.org/10.1021/acsomega.2c00296
ACS Omega 2022, 7, 11293−11304

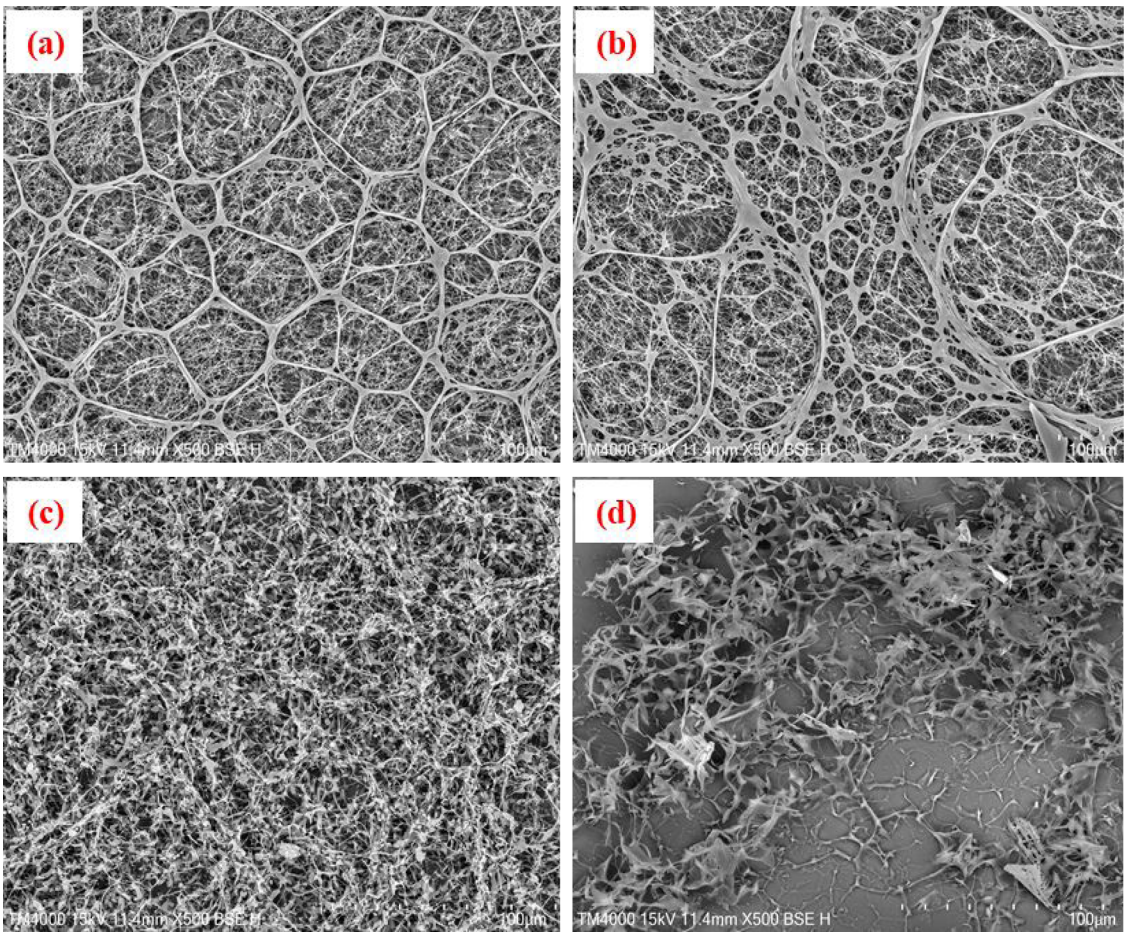

Figure 10. Effect of shearing on polymer morphology. (a) Initial sample of SRP; (b) Sample of SRP after shearing; (c) Initial sample of PHPAM; (d) Sample of PHPAM after shearing.

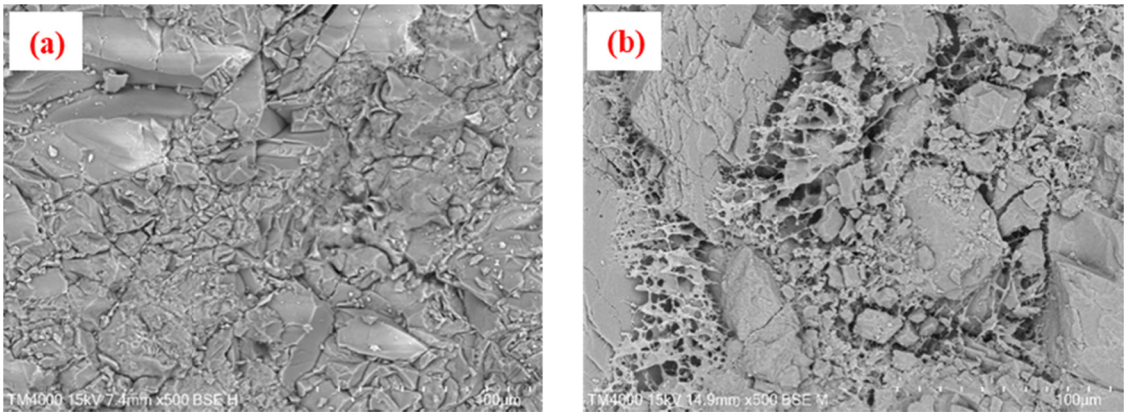

Figure 11. Physical drawing of the polymer adsorption plug. (a) Original state of the surface of the natural core; (b) surface state of the natural core after polymer flooding.

occupy adsorption sites on the rock surface. Consequently, a larger amount of surface area is available for polymer molecules, corresponding to a higher level of adsorption.

The adsorption of polymers in the porous media of hydrophilic rocks can decrease the selectivity of rock permeability. The decrease in permeability caused by polymer adsorption can be explained by the "geometric" effect, that is, the decrease in the pore and throat size caused by the polymer adsorption layer changing the size of the porous medium (restricting the pore throat). When the core permeability is lower than 20 mD and the thickness of the polymer adsorption layer is greater than 0.5 μm, the core is completely blocked. Because polymer adsorption is irreversible, severe adsorption can occur.[36,37] If the adsorbed polymer occupies a large pore volume, it is difficult to recover a substantial amount of oil. In addition, the formation permeability decreases, resulting in lower recovery.

Figure 11a shows the original state of the surface of the natural core, and Figure 11b shows the surface state of the natural core after polymer flooding. SRP is a highly viscous fluid. When SRP

https://doi.org/10.1021/acsomega.2c00296
ACS Omega 2022, 7, 11293−11304

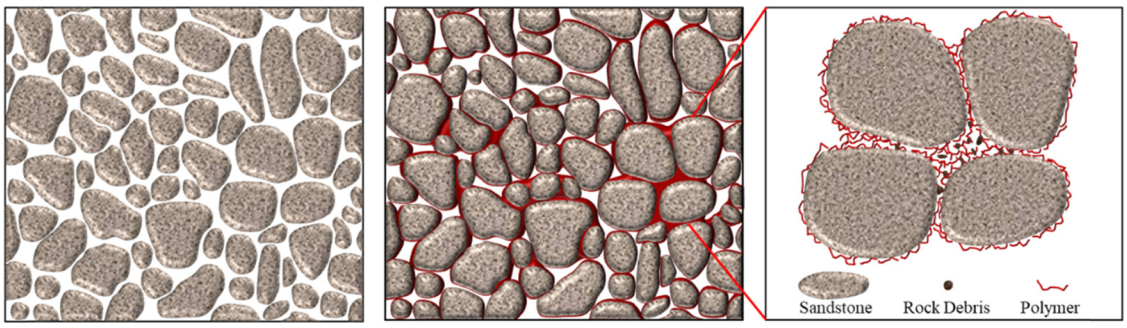

Figure 12. Schematic of the polymer adsorption blocking mechanism.

passes through the natural core, the polymer is not only adsorbed on the pore surface of the rock but also connects the two sides of the pore. Consequently, a polymer molecular network is formed in the pore, and the pore space is divided into smaller intervals. Moreover, because of the loose cementation of the core, the fine sand particles formed after the broken core are carried by the polymer until they block the middle or outlet end of the core,[38,39] resulting in a significant decrease in the size of the hole roar. Figure 12 schematically illustrates the adsorption, bridging, and sand-carrying effects of the polymer blockage.

CONCLUSIONS

(1) According to the polymer flooding experiments, the lower limit of permeability of the cores displaced by the medium-molecular SRP solution is 20−40 mD. SRP exhibits higher injectability and adsorption retention than those of the PHPAM.

(2) The resistance coefficient and the residual resistance coefficient in the natural core flooding experiment are approximately two and three times those of the artificial core for a given permeability.

(3) For cores with permeabilities greater than 100 mD, the SRP concentration can be more than 900 mg/L. However, for cores with low permeabilities of approximately 50 mD, the SRP concentration must be less than 900 mg/L.

(4) According to polymer adsorption experiments, the static adsorption amounts of the three polymers are steady when the standing time exceeds 36 h. The liquid−solid ratio is a key factor that influences the upper limit of the static adsorption capacity of the SRP. When the SRP concentration is 900 mg/L, the static adsorption amount (3.56 mg/g) is high and approximately 2−5 times the dynamic adsorption amount.

(5) The injection capacity of the SRP decreases owing to the following reasons: the molecular gyration radius of the SRP is 0.19 μm, and the permeability can be decreased by 43.7% for Daqing Oilfield with an average permeability of 100 mD. Moreover, considerable aggregation occurs, and the size of the aggregated polymer group can reach 5−10 μm, considerably exceeding the pore radius of the rock. The SRP exhibits a high shear resistance, maintains a high bonding strength, and is not easily damaged. Moreover, the polymer carries fine sand particles, which block the middle or outlet end of the core, resulting in a significant decrease in the size of the pore roar.

AUTHOR INFORMATION

Corresponding Author

Liguo Zhong − *Unconventional Petroleum Research Institute, China University of Petroleum Beijing, 102249 Beijing City, China;* orcid.org/0000-0001-9230-6995; Email: zhongliguo007@163.com

Authors

Tongchun Hao − *Unconventional Petroleum Research Institute, China University of Petroleum Beijing, 102249 Beijing City, China;* orcid.org/0000-0002-3179-5446

Jianbin Liu − *Unconventional Petroleum Research Institute, China University of Petroleum Beijing, 102249 Beijing City, China*

Hongyu Sun − *Unconventional Petroleum Research Institute, China University of Petroleum Beijing, 102249 Beijing City, China*

Tianyin Zhu − *Unconventional Petroleum Research Institute, China University of Petroleum Beijing, 102249 Beijing City, China*

Hailong Zhang − *Downhole Operation Branch of Daqing Oilfield Co., LTD, 163458 Daqing, Hei Longjiang Province, China*

Shaojie Wu − *Downhole Operation Branch of Daqing Oilfield Co., LTD, 163458 Daqing, Hei Longjiang Province, China*

Complete contact information is available at: https://pubs.acs.org/10.1021/acsomega.2c00296

Notes

The authors declare no competing financial interest.

ACKNOWLEDGMENTS

We would like to express our heartfelt thanks to the Science and Technology Project "Study on the Formation and Identification Technology of High Pressure Wells after Fracturing" from the Downhole Operation Branch of Daqing Oilfield Co., Ltd for the financial support for this work.

REFERENCES

(1) Liao, G. Z.; Wang, Q.; Wang, H. Z.; Liu, W. D.; Wang, Z. M. Chemical flooding development status and prospect. *Acta Pet. Sin.* **2017**, *38*, 196−207.

(2) Lu, X. G.; Hu, G. B.; Cao, W. J.; Su, X. Effect of polymer retention on enhanced oil recovery by chemical flooding. *Pet. Geol. Oilfield Dev. Daqing* **2016**, *35*, 99−105.

(3) Shen, P. P.; Yuan, S. Y.; Deng, B. R.; Song, J.; Sen, K. Y. Influence factors of oil displacement efficiency and sweep efficiency in chemical flooding. *Pet. Explor. Dev.* **2004**, *31*, 1−4.

(4) Abidin, A. Z.; Puspasari, T.; Nugroho, W. A. Polymers for enhanced oil recovery technology. *Procedia Chem.* **2012**, *4*, 11−16.

(5) Brantson, E. T.; Ju, B. S.; Appau, P. O.; Akwensi, P. H.; Peprah, G. A.; Liu, N. N.; Aphu, E. S.; Boah, E. A.; Borsah, A. A. Development of hybrid low salinity water polymer flooding numerical reservoir simulator and smart proxy model for chemical enhanced oil recovery (CEOR). *J. Pet. Sci. Eng.* **2020**, *187*, No. 106751.
(6) Li, D. S.; Zhou, J. X.; Ni, F. T.; Zhang, J. C.; Sun, X. Q.; Cheng, L. J. Research on Sewage Based Polymer Flooding for High Temperature and High Salinity Oil Reservoir in South Dagang Oilfield. *Pet. Geol. Oilfield Dev. Daqing* **2007**, *26*, 100−104.
(7) Lin, Y. J.; Liu, B.; Tan, Y.; Bai, Y. Research on the polymer flooding test in the eastern area of block Jin 16, Liaohe oil field. *Pet. Geol. Recovery Effic.* **1996**, *3*, 42−46.
(8) Sun, H. Q. Application of pilot test for well pattern adjusting heterogeneous combination flooding after polymer flooding: A case of Zhongyiqu Ng3 block, Gudao Oilfield. *Pet. Geol. Recovery Effic.* **2014**, *21*, 1−4.
(9) Al-Hajri, S.; Mahmood, S. M.; Abdulelah, H.; Akbari, S. An overview on polymer retention in porous media. *Energies* **2018**, *11*, 2751.
(10) Chen, H. X.; Gao, J. C.; Tang, X. X.; Cui, G.; Zhu, K. Cause analysis of high injection pressure and measure of augmented injection in polymer injectors of SZ 36-1 oilfield. *China Offshore Oil Gas* **2011**, *23*, 189−192.
(11) Chen, H. X.; Liu, Y. G.; Feng, Y. T.; Pang, M.; Meng, X. H.; Yang, B. Scaling Mechanism of Polymer-contained Sewage Reinjection in Polymer Flooding Offshore Oilfields. *Oilfield Chem.* **2018**, *35*, 691−697.
(12) Kang, W. L.; Wang, T. Y.; Zhang, H. W.; Hou, X. Y.; Zhang, X. F.; Zhu, T. Y.; Chen, C.; Yang, H. B. A dynamic scale location monitor method to predict oilfield blockage during water flooding. *J. Pet. Sci. Eng.* **2020**, *191*, No. 107168.
(13) Khalili Nezhad, S. S.; Cheraghian, G. Mechanisms behind injecting the combination of nano-clay particles and polymer solution for enhanced oil recovery. *Appl. Nanosci.* **2016**, *6*, 923−931.
(14) Cheraghian, G.; Khalili Nezhad, S. S.; Bazgir, S. Improvement of thermal stability of polyacryl amide solution used as a nano-fluid in enhanced oil recovery process by nanoclay. *Int. J. Nanosci. Nanotechnol.* **2015**, *11*, 201−208.
(15) Hibbeler, J.; Garcia, T.; Chavez, N. An Integrated Long-Term Solution for Migratory Fines Damage. *Soc. Pet. Eng.* **2003**, DOI: 10.2118/81017-MS.
(16) Alfazazi, U.; Thomas, N. C.; Alameri, W.; Al-Shalabi, W. E. Experimental investigation of polymer injectivity and retention under harsh carbonate reservoir conditions. *J. Pet. Sci. Eng.* **2020**, *192*, No. 107262.
(17) Dong, W. T.; Zhang, D.; Wang, K. L.; Qiu, Y. Investigation on degradation mechanism of polymer blockages in unconsolidated sandstone reservoirs. *e-Polymers* **2020**, *20*, 55−60.
(18) Yang, H. B.; Iqbal, W. M.; Lashariet, A. Z.; Cao, C. X.; Tang, X. C.; Kang, W. L. Experimental research on amphiphilic polymer/organic chromium gel for high salinity reservoirs. *Colloids Surf., A* **2019**, *582*, No. 123900.
(19) Yang, H. B.; Shao, S.; Zhu, T. Y.; Chen, C.; Liu, S. R.; Zhou, B. B.; Hou, X. Y.; Zhang, Y.; Kang, W. L. Shear resistance performance of low elastic polymer microspheres used for conformance control treatment. *J. Ind. Eng. Chem.* **2019**, *79*, 295−306.
(20) Wang, F.; Yang, H. B.; Jiang, H. Z.; Kang, X.; Hou, X. Y.; Wang, T. Y.; Zhou, B. B.; Sarsenbekuly, B.; Kang, W. L. Formation mechanism and location distribution of blockage during polymer flooding. *J. Pet. Sci. Eng.* **2020**, *194*, No. 107503.
(21) Liao, Z. W.; Zhou, H. G.; Graciaa, A.; Chrostowska, A.; Creux, P.; Geng, A. S. Adsorption/occlusion characteristics of asphaltenes: some implication for asphaltene structural features. *Energy Fuels* **2005**, *19*, 180−186.
(22) Lee, K. S. Effects of polymer adsorption on the oil recovery during polymer flooding processes. *Pet. Sci. Technol.* **2010**, *28*, 351−359.
(23) Lu, D. Y.; Meng, X. H.; Wu, W.; Zhou, J. Y. Analysis on the plugging mechanism and the removal technology for polymer flooding blocks in Bohai sea. *China Offshore Oil Gas* **2016**, *28*, 98−103.
(24) Li, Q. J.; Prigiobbe, V. Numerical simulations of the migration of fine particles through porous media. *Transp. Porous Media* **2018**, *122*, 745−759.
(25) Houchin, L. R.; Hudson, L. M. The Prediction, Evaluation, and Treatment of Formation Damage Caused by Organic Deposition. *Soc. Pet. Eng.* **1986**, DOI: 10.2118/14818-MS.
(26) Wood, J. M.; Spark, I. S. C. Microbially Induced Formation Damage in Oilfield Reservoirs. *Soc. Pet. Eng.* **2000**, DOI: 10.2118/58750-MS.
(27) Qu, H. M.; Wang, P. F.; Wu, Q.; Luo, Y.; Dai, Q.; Wang, H. Y. Development and field application of a new amphoteric bactericide for polymer-bearing waste water. *Complex Hydrocarbon Reservoirs* **2019**, *12*, 84−88.
(28) Xie, K.; Lu, X. G.; Li, Q.; Liang, W. D.; Yu, Q. Analysis of reservoir applicability of hydrophobically associating polymer. *SPE J.* **2016**, *21*, 1−9.
(29) Xie, K.; Lu, X. G.; Jiang, W. D.; Li, Q. Reservoir adaptability and mechanism of salt-resistant polymer. *J. China Univ. Pet., Ed. Nat. Sci.* **2017**, *41*, 144−153.
(30) Xie, K.; Cao, B.; Lu, X. G.; Jiang, W. D.; Zhang, Y. B.; Li, Q.; Song, K. P.; Liu, J. X.; Wang, W.; Lv, J. L.; Na, R. S. Matching between the diameter of the aggregates of hydrophobically associating polymers and reservoir pore-throat size during polymer flooding in an offshore oilfield. *J. Pet. Sci. Eng.* **2019**, *177*, 558−569.
(31) Guo, H. How to select polymer molecular weight and concentration to avoid blocking in polymer flooding. *Soc. Pet. Eng.* **2017**, DOI: 10.2118/189255-MS.
(32) Zhang, G. Y.; Seright, R. S. Effect of Concentration on HPAM Retention in Porous Media. *SPE J.* **2014**, *19*, 373−380.
(33) Manichand, R. N.; Seright, R. S. Field vs. Laboratory polymer-retention values for a polymer flood in the tambaredjo field. *SPE Reservoir Eval. Eng.* **2014**, *17*, 314−325.
(34) Zhang, Z. Y.; Jiang, H. Q.; Ding, M. A. Experimental study on polymer injection capacity. *J. Exp. Mech.* **2009**, *24*, 8−12.
(35) Yan, W. H.; Liu, W. D.; Luo, L. T.; Xu, K. Study on Hydrodynamic Size of Polymer Solution. *Sci. Technol. Eng.* **2014**, *14*, 182−185.
(36) Lee, J. J.; Fuller, G. G. Adsorption and desorption of flexible polymer chains in flowing systems. *J. Colloid Interface Sci.* **1985**, *103*, 569−577.
(37) Zhu, S. J.; Ye, Z. B.; Liu, Z. Z.; Chen, Z. H.; Li, J.; Xiang, Z. P. Adsorption Characteristics of Polymer Solutions on Media Surfaces and Their Main Influencing Factors. *Polymer* **2021**, *13*, 1774.
(38) Valdya, R. N.; Fogler, H. S. Fines Migration and Formation Damage: Influence of pH and Ion Exchange. *SPE Prod. Eng.* **1992**, *7*, 325−330.
(39) Wu, X. C.; Han, D. K.; Lu, X. G.; Ye, Y. Z.; Sun, Z. Oil displacing mechanism of soft micro particle dispersion in porous media. *Earth Sci.* **2017**, *42*, 1348−1355.

https://doi.org/10.1021/acsomega.2c00296
ACS Omega 2022, 7, 11293−11304